Journal of Molecular Structure 1198 (2019) 126915

Contents lists available at ScienceDirect

Journal of Molecular Structure

journal homepage: http://www.elsevier.com/locate/molstruc

Facile synthesis of new quinazolinone benzamides as potent tyrosinase inhibitors: Comparative spectroscopic and molecular docking studies

Prasad G. Mahajan [a, 1], Nilam C. Dige [b, 1], Balasaheb D. Vanjare [a], Hussain Raza [b], Mubashir Hassan [c], Sung-Yum Seo [b, **], Chong- Hyeak Kim [d], Ki Hwan Lee [a, *]

[a] Department of Chemistry, Kongju National University, Gongju, Chungnam, 32588, Republic of Korea
[b] Department of Biological Sciences, Kongju National University, Gongju, Chungnam, 32588, Republic of Korea
[c] Institute of Molecular Biology and Biotechnology, The University of Lahore, Defence Road, Lahore, 54590, Pakistan
[d] Center for Chemical Analysis, Korea Research Institute of Chemical Technology, Yuseong, Daejeon, 34114, Republic of Korea

ARTICLE INFO

Article history:
Received 31 May 2019
Received in revised form
6 August 2019
Accepted 8 August 2019
Available online 9 August 2019

Keywords:
Quinazolinone benzamides
Spectroscopic properties
Tyrosinase inhibition
Lipinski's rule
Drug score
Molecular docking

ABSTRACT

The simple reaction approach has been designed and utilized for the synthesis of quinazolinone benzamides **4a-4h** using isatoic anhydride, *m*-Anisic hydrazide and various aldehydes. The formation of target compounds was confirmed by spectral characterization techniques such as IR, NMR, Mass and elemental analysis. The spectrophotometric investigations based on absorption and fluorescence outputs denote distinctive properties such as molar extinction coefficient, fluorescence emission, fluorescence lifetime, quantum yield and Stokes shift for compounds **4a-4h** in three different solvents. Along with spectroscopic studies, synthesized compounds **4a-4h** were tested for bioevaluation against tyrosinase inhibitory activity. Pleasingly, all compounds displayed lower IC_{50} values (0.006 ± 0.074 to 1.609 ± 0.324 μM) than standard kojic acid (16.832 ± 1.162 μM) against tyrosinase inhibition. The comparative spectrophotometric properties, *in vitro* and *in silico* analysis suggest that compounds **4d** and **4f** have significant absorption and fluorescence properties in addition to extremely low IC_{50} values as potent tyrosinase inhibitors.

1. Introduction

Recently, researchers are engaged in designing, synthesizing and exploring various nitrogen containing organic heterocyclic compounds which have medicinal importance. Amongst the variety of compounds from huge library of heterocycles, quinazolinones are crucial and beneficial compounds as far as design and development of medicines in pharmaceutical industries [1,2]. It is well known that quinazolinones are found in structural core of various bioactive natural products such as cottoquinazoline, millitarinone, etc [3,4]. Quinazolinones and their derivatives were successfully exploited for the investigation of their biological activities which covers a broad range of antibacterial, antiviral, analgesic, anti-inflammatory, anticancer, antidiabetic and anti-tussive effects [5–11]. Mainly, quinazolin-4(*1H*)-ones and quinazoline-4(*3H*)-ones are the inter-convertible forms of quinazolinone family and can be useful as primitive template of target compound in the development of drug discovery.

Quinazolinone representative structure is given as Fig. 1a. Few research reports witnessed that different quinazolinone structures were claimed for the investigation of sedative drugs (Fig. 1b), thyroid-stimulating hormone receptor agonist (Fig. 1c) and Tankyrase inhibitor (Fig. 1d). In addition to the biological applications, quinazolinones show remarkable spectroscopic properties such as high molar extinction coefficient, absorption, fluorescence emission, fluorescence quantum yield, Stokes shift and fluorescence lifetime [12–14]. Nowadays, such organic compounds possessing exceptionally good optical properties have gained much more attention and challenge in the scientific field which mainly deal with organic light emitting diodes, sensors, cell imaging and optoelectronics [15–18]. The variety of synthetic approaches has been used by organic chemists for the synthesis of quinazolinones. During the course of design and synthesis of quinazolinone derivatives in present studies, the attentions were focused towards

* Corresponding author.
** Corresponding author.
E-mail addresses: dnalove@kongju.ac.kr (S.-Y. Seo), khlee@kongju.ac.kr (K.H. Lee).
[1] These authors have equal contributions for this research work.

https://doi.org/10.1016/j.molstruc.2019.126915
0022-2860/

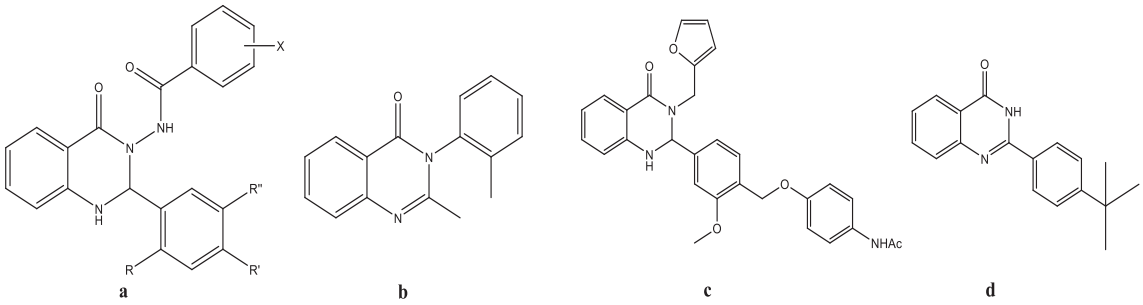

Fig. 1. Representative structure of quinazolinone (a) and its examples (b–d).

the ease of synthetic approach, high yield of products, easy to reproduce the synthetic protocol and obtained products can be advantageous in bio-estimation against different activities.

Tyrosinase is a copper containing metalloenzyme widely spread over the skin in human body. The tyrosinase enzyme plays a crucial role in production, functioning and mechanism of melanin along with control on pigments in animal and human body [19,20]. The abnormal accretion of melanin in human body is responsible for the major skin diseases, hyperpigmentation, Parkinson's disease and Huntington's disease [19–23]. Tyrosinase actively participate in the oxidation process of dopamine to dopaquinones. The excess quantity of dopaquinones may produce harm to neurological system and simultaneously damage cells [20]. Therefore, functioning of melanin in human body through inhibition of tyrosinase enzyme is essential for normal and healthy growth. Such scenario encourages the researchers for the development of significant structural templates that can be useful in drug design and served as inhibitor for excess tyrosinase production in the human body. Literature review indicates that various organic compounds with and without heterocyclic structural cores were successfully investigated as potent tyrosinase inhibitors namely kojic acid, arbutin, ellagic acid, L-ascorbic acid, flavones, coumarins, azole, thiazolidine, chalcones, xanthene's, analogues of carboxylic acids and aldehydes, substituted phenols, pyridines and piperidines [24–26]. Therefore, considering the multiutility of quinazolinone derivatives in optical as well as pharmaceutical applications, we envisioned our experimental plan with the aim of design and synthesis of quinazolinone benzamides followed by their spectroscopic investigation and screening of potent inhibitory activity against tyrosinase enzyme.

In the present research work, we have synthesized new derivatives of quinazolinone benzamides using multicomponent reaction approach *via* sequential addition of isatoic anhydride, *m*-Anisic hydrazide and various aldehydes in the presence of *p*-toluene sulfonic acid (*p*-TSA) in water: ethanol (6:4 *v:v*) at ultrasonic conditions for specific reaction time. The quinazolinone derivatives were successfully synthesized and fully characterized by spectral techniques. The advantage of present investigations includes practical simplicity, use of green solvents, higher yield of products, easy isolation of products, discriminating spectroscopic properties based on absorption and fluorescence studies and most important potent bio-evaluation against tyrosinase enzyme. Pleasingly, all synthesized quinazolinone derivatives were found to be potentially active tyrosinase inhibitors as compared to standard kojic acid.

2. Experimental section

2.1. Chemistry

2.1.1. Materials

Various substituted aldehydes, isatoic anhydride, *m*-Anisic hydrazide and *p*-Toluene sulfonic acid (*p*-TSA) were purchased from Sigma-Aldrich, Korea and used as received without further purification. The methanol, chloroform and dichloromethane (DCM) were procured from Samchun Chemicals, Korea and used after distillation.

2.1.2. Methods

The melting point of synthesized compounds were recorded on Digimelt (SRS, USA) melting point apparatus. The spectral techniques such as IR, NMR and Mass analysis were procured to analyze the structure and formation of products (**4a-4h**). IR spectra were recorded on a Frontier IR Perkin–Elmer spectrophotometer. NMR spectra were scanned on a Bruker AC-400 spectrometer using tetramethylsilane as an internal standard. Mass spectra were obtained using Shimadzu QP 2010 GCMS (Japan) spectrophotometer. UV–visible absorption spectra of newly synthesized quinazolinone benzamides **4a-4h** were scanned on a Shimadzu Spectrophotometer in different solvents such as methanol, chloroform and DCM at each of 1 μM concentration. The fluorescence emission spectra of **4a-4h** were inspected on FS-2 fluorescence spectrophotometer (Scinco, Korea) in individual solvent at mentioned concentration. The respective excitation wavelength was used to examine the fluorescence emission spectrum of each compound in said solvents. The fluorescence lifetime values of **4a-4h** were obtained by triggering the respective solutions at specific excitation wavelength on Time Correlated Single Photon Counting (TCSPC) spectrophotometer (HORIBAiHR320) having time correlation of 0.0548 ns per channel. The fluorescence quantum yield (ϕ_f) for all synthesized quinazolinones **4a-4h** were estimated at 1 μM concentration with quinine sulphate as reference ($\phi_f = 0.58$) and using following equation (1) [27,28].

$$\phi_f = \phi_{f\,(ref)} \frac{F_P\, A_{ref} n^2}{F_{ref}\, A_P n_{ref}^2} \quad (1)$$

where, ϕ_f and $\phi_{f\,(ref)}$ denotes the fluorescence quantum yields of individual compound **4a-4h** and reference quinine sulphate, respectively. The areas under the curve of emission spectrum of compound **4a-4h** and quinine sulphate are given as F_P and F_{ref}, respectively. While, A_{ref}, A_P, n and n_{ref} are the absorbance of quinine sulphate, absorbance of compound **4a-4h**, refractive index of solvent used to dissolve the compound **4a-4h** and quinine sulphate, respectively.

2.1.3. General procedure for synthesis of quinazolinone benzamides 4a-4h

The 50 mL round bottom flask was equipped with an equimolar amount of isatoic anhydride (1 mmol) and *m*-Anisic hydrazide (1 mmol) in 10 mL of water: ethanol (6:4 *v/v*) mixed solvent and *p*-TSA (10 mol %). The resultant reaction mixture was sonicated till the completion of reaction. Then, respective aldehyde (1 mmol) was

sequentially added to the same reaction mixture. The reaction mixture was further sonicated, and the progress of reaction was monitored by thin layer chromatography (TLC) for specific reaction time. After completion of reaction, the product was isolated by simple filtration method and washed with ethanol. Scheme 1 illustrates the synthetic route for quinazolinone benzamides **4a-4h**. The structures of final products **4a-4h** shown in Fig. 2. Table 1 represents substituents on designed molecule, time required for completion of each reaction to form **4a-4h** and obtained product yield.

Table 1
Different substituents, reaction time and product yield for newly synthesized quinazolinone benzamides (**4a-4h**).

Entry	R	R′	R″	Time (h)	Yield (%)
4a	OH	H	H	2.8	79
4b	H	H	H	3.2	88
4c	OH	H	I	2.1	87
4d	H	F	H	2.3	86
4e	H	Br	H	2.1	82
4f	H	CH_3	H	3.6	78
4g	H	OCH_3	H	3.1	83
4h	H	NO_2	H	2.8	87

2.1.3.1. Spectral characteristics of synthesized quinazolinone benzamides (4a-4h)

2.1.3.1.1. N-(2-(2-hydroxyphenyl)-4-oxo-1,2-dihydroquinazolin-3(4H)-yl)-3-methoxybenzamide (4a). This reaction was performed by reaction between isatoic anhydride, *m*-Anisic hydrazide and salicylaldehyde. White powder; M.P.: 152 °C; IR (**ESI,** Fig. S1): 3465, 3353, 3148, 3011, 2298, 1593, 1529, 1452, 1395, 1357, 1283, 1192, 1118, 967, 913, 904, 817, 735, 682 cm^{-1}; ^{1}H NMR(**ESI,** Fig. S2 and 400 MHz, DMSO-d_6): δ 12.10 (s, 1H, −NH), 11.74 (s, 1H, −NH), 10.56 (s, 1H, −OH), 8.64 (s, 1H), 7.97–7.98 (m, 2H), 7.72–7.75 (m, 1H), 7.18–7.26 (m, 3H), 7.12–7.18 (m, 2H), 6.85–6.91 (m, 3H), 6.72–6.73 (m,1H), 3.74 (s, 3H, $-OCH_3$) ppm; ^{13}C NMR (**ESI,** Fig. S3**,** 100 MHz, DMSO-d_6): δ 160.34, 152.61, 151.86, 147.56, 146.50, 141.87, 137.40, 129.40, 123.98, 118.74, 117.74, 115.78, 112.61, 110.74, 55.98 ppm; MS (EI) (**ESI,** Fig. S4): 390.3 (M+1), *m/z*. Elemental analysis calcd (%) for $C_{22}H_{19}N_3O_4$: C 67.86; H 4.92; N 10.79; O 16.43; found: C 67.84; H 4.91; N 10.81; O 16.44.

2.1.3.1.2. 3-Methoxy-N-(4-oxo-2-phenyl-1,2-dihydroquinazolin-3(4H)-yl)benzamide (4b). Isatoic anhydride, *m*-Anisic hydrazide and benzaldehyde were used as starting materials for this reaction. Cream coloured powder; M.P.: 110 °C; IR (**ESI,** Fig. S5): 3464, 3352, 3154, 3021, 1726, 1612, 1594, 1530, 1485, 1451, 1395, 1358, 1323, 1286, 1202, 1192, 1142, 1134, 1119, 967, 913, 903, 818, 751, 682 cm^{-1}; ^{1}H NMR(**ESI,** Fig. S6, 400 MHz, DMSO-d_6): δ 11.81 (s, 1H, −NH), 11.73 (s, 1H, −NH), 8.48 (s, 1H), 7.16–7.94 (m,13H), 3.85 (s, 3H, $-OCH_3$) ppm; ^{13}C NMR (**ESI,** Fig. S7**,** 100 MHz, DMSO-d_6): δ 178.93, 160.33, 148.64, 148.23, 147.42, 141.94, 137.27, 134.70, 130.45, 130.04, 129.22, 128.49, 127.46, 124.15, 120.43, 118.06, 115.77, 114.14, 113.40, 11,062, 55.90 ppm; MS (EI) (**ESI,** Fig. S8): 374.3 (M+1), *m/z*. Elemental analysis calcd (%) for $C_{22}H_{19}N_3O_3$: C 70.76; H 5.13; N 11.25; O 12.86; found: C 70.77; H 5.10; N 11.26; O 12.87.

2.1.3.1.3. N-(2-(2-hydroxy-5-iodophenyl)-4-oxo-1,2-dihydroquinazolin-3(4H)-yl)-3-methoxybenzamide (4c). This reaction was carried out by using isatoic anhydride, *m*-Anisic hydrazide and 5-Iodo salicylaldehyde. White powder; M.P.: 181 °C; IR (**ESI,** Fig. S9): 3465, 3352, 3154, 3022, 1647, 1590, 1527, 1477, 1463, 1356, 1282, 1202, 1192, 1142, 1134, 1119, 1036, 967, 903, 816, 737, 682 cm^{-1}; ^{1}H NMR(**ESI,** Fig. S10**,** 400 MHz, DMSO-d_6): δ 11.09 (s, 1H, −NH), 9.12 (s, 1H, −NH), 8.46 (s, 1H, −OH), 7.59–7.61 (m, 1H), 7.54–7.56 (m, 2H), 7.50 (s, 1H), 7.43–7.46 (t, 2H, J = 10.8 & 4 MHz),

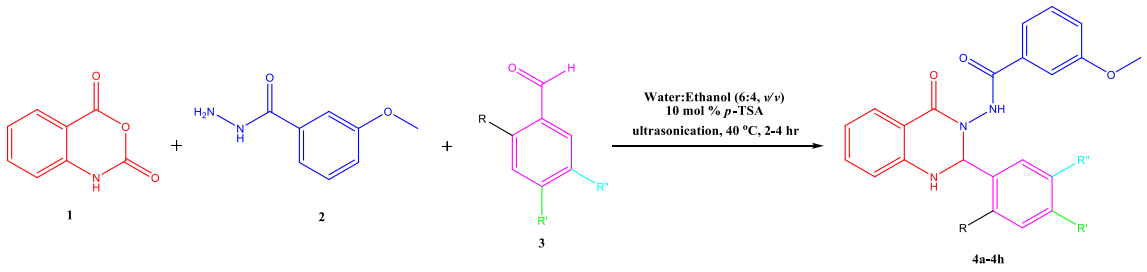

Scheme 1. Synthetic route for quinazolinone benzamides (**4a-4h**).

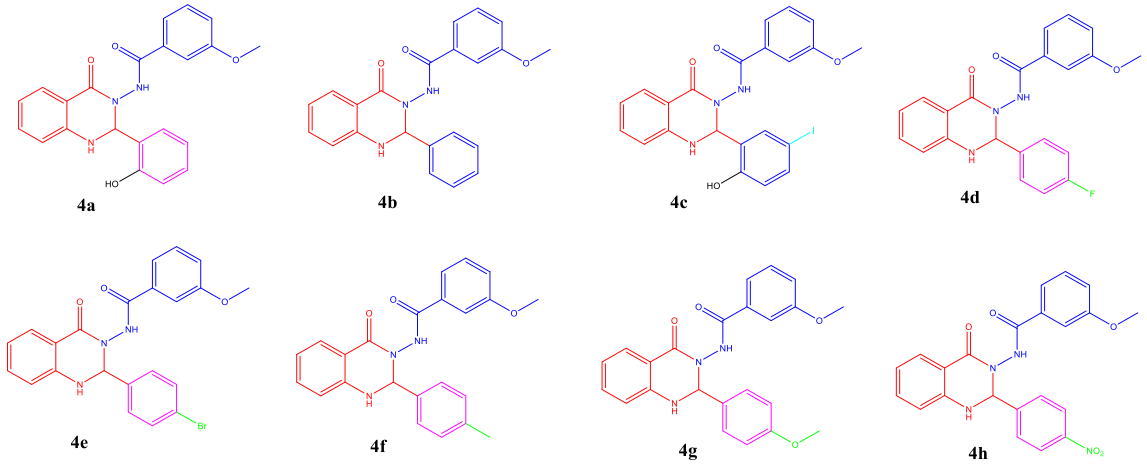

Fig. 2. Structures of newly synthesized quinazolinone benzamides (**4a-4h**).

7.38–7.39 (d, 3H, $J = 4$ Hz), 7.14–7.17 (m, 1H), 7.09 (s, 1H), 6.85–6.86 (d, 1H), 3.91 (s, 3H, $-OCH_3$) ppm; ^{13}C NMR(**ESI,** Fig. S11**,** 100 MHz, DMSO-d_6): δ 162.66, 159.75, 149.55, 135.72, 130.10, 129.32, 121.06, 120.27, 117.83, 113.37, 111.62, 55.87, 44.49, 12.89 ppm; MS (EI) (**ESI,** Fig. S12): 516.2 (M+1), *m/z*. Elemental analysis calcd (%) for $C_{22}H_{18}IN_3O_4$: C 51.28; H 3.52; I 24.63, N 8.15; O 12.42; found: C 51.25; H 3.53; I 24.65, N 8.14; O 12.43.

2.1.3.1.4. N-(2-(4-fluorophenyl)-4-oxo-1,2-dihydroquinazolin-3(4H)-yl)-3-methoxybenzamide (4d). The reaction between isatoic anhydride, *m*-Anisic hydrazide and 4-fluoro benzaldehyde as starting materials offered compound **4d** as final product. Cream coloured powder; M.P.: 134 °C; IR(**ESI,** Fig. S13): 3445, 3178, 3022, 1726, 1640, 1529, 1395, 1284, 1202, 1192, 1142, 1133, 1120, 1042, 967, 913, 903, 818, 750, 690, 6982 cm^{-1}; ^{1}H NMR(**ESI,** Fig. S14, 400 MHz, DMSO-d_6): δ 9.23 (s, 1H, −NH), 8.37 (s, 1H, −NH), 7.81 (s, 1H), 7.59–7.62 (m, 1H), 7.40–7.43 (t, 3H, $J = 4$ & 8 MHz), 7.23–7.26 (t, 1H, $J = 4$ & 8 MHz), 7.09–7.16 (m, 4H), 6.73–6.74 (m, 1H), 6.46–6.48 (m, 1H), 3.90 (s, 3H, $-OCH_3$) ppm; ^{13}C NMR(**ESI,** Fig. S15**,** 100 MHz, DMSO-d_6): δ 173.51, 149.41, 130.05, 129.29, 118.89, 117.98, 112.98, 112.10, 55.80, 40.57, 29.83 ppm; MS (EI) (**ESI,** Fig. S16): 392.3 (M+1), *m/z*. Elemental analysis calcd (%) for $C_{22}H_{18}FN_3O_3$: C 67.51; H 4.64; F 4.85, N 10.74; O 12.26; found: C 67.52; H 4.62; F 4.86, N 10.72; O 12.28.

2.1.3.1.5. N-(2-(4-bromophenyl)-4-oxo-1,2-dihydroquinazolin-3(4H)-yl)-3-methoxybenzamide (4e). The compound **4e** was synthesized by using isatoic anhydride, *m*-Anisic hydrazide and 4-bromo benzaldehyde. White powder; M.P.: 154 °C; IR(**ESI,** Fig. S17): 3445, 3169, 3022, 2297, 1726, 1638, 1582, 1531, 1509, 1486, 1395, 1361, 1284, 1202, 1192, 1142, 1133, 1120, 1048, 967, 913, 903, 819, 749, 682 cm^{-1}; ^{1}H NMR(**ESI,** Fig. S18, 400 MHz, DMSO-d_6): δ 9.20 (s, 1H, −NH), 8.35 (s, 1H, −NH), 7.68 (s, 1H), 7.57–7.59 (m, 4H), 7.50 (s,1H), 7.41–7.47 (m, 4H), 7.12–7.15 (m, 3H), 3.91 (s, 3H, $-OCH_3$) ppm; ^{13}C NMR(**ESI,** Fig. S19**,** 100 MHz, DMSO-d_6): δ 179.95, 166.45, 129.41, 115.82, 59.14, 55.49, 31.90, 29.66, 29.33, 23.78, 22.67, 14.15 ppm; MS (EI) (**ESI,** Fig. S20): 455.2 (M+3), *m/z*. Elemental analysis calcd (%) for $C_{22}H_{18}BrN_3O_3$: C 58.43; H 4.01; Br 17.66, N 9.27; O 10.63; found: C 58.42; H 4.01; Br 17.67, N 9.29; O 10.61.

2.1.3.1.6. 3-Methoxy-N-(4-oxo-2-p-tolyl-1,2-dihydroquinazolin-3(4H)-yl)benzamide (4f). This reaction was performed by reaction between isatoic anhydride, *m*-Anisic hydrazide and *p*-Tolualdehyde gave us compound **4f**. White powder; M.P.: 105 °C; IR(**ESI,** Fig. S21): 3446, 3226, 3022, 2961, 2299, 1637, 1602, 1580, 1511, 1487, 1449, 1395, 1282, 1202, 1192, 1142, 1133, 1120, 1046, 967, 903, 809, 749, 682 cm^{-1}; ^{1}H NMR(**ESI,** Fig. S22**,** 400 MHz, DMSO-d_6): δ 11.75 (s, 1H, −NH), 10.37 (s, 1H, −NH), 8.43 (s, 1H), 7.10–7.65 (s, 11H), 6.13 (s, 1H), 3.84 (s, 3H, $-OCH_3$), 2.36 (s, 3H, $-CH_3$) ppm; ^{13}C NMR(**ESI,** Fig. S23**,** 100 MHz, DMSO-d_6): δ 174.57, 165.71, 163.41, 159.27, 154.91, 148.49, 139.19, 135.48, 134.29, 131.97, 130.11, 129.25, 128.68, 127.61, 126.18, 120.40, 118.32, 115.03, 114.18, 113.38, 112.96, 74.93, 55.49, 21.61, 21.19 ppm; MS (EI) (**ESI,** Fig. S24): 388.3 (M+1), *m/z*. Elemental analysis calcd (%) for $C_{23}H_{21}N_3O_3$: C 71.30; H 5.46; N 10.85; O 12.39; found: C 71.28; H 5.45; N 10.86; O 12.41.

2.1.3.1.7. 3-Methoxy-N-(2-(4-methoxyphenyl)-4-oxo-1,2-dihydroquinazolin-3(4H)-yl)benzamide(4g). The synthesis of final compound **4g** was achieved through reaction between isatoic anhydride, *m*-Anisic hydrazide and *p*-Anisaldehyde as starting materials offered compound **4d** as final product. Brown powder; M.P.: 112 °C; IR(**ESI,** Fig. S25): 3445, 3225, 3022, 2961, 2298, 2102, 1726, 1640, 1582, 1395, 1283, 1202, 1192, 1142, 1133, 697, 903, 818, 750, 682 cm^{-1}; ^{1}H NMR(**ESI,** Fig. S26, 400 MHz, DMSO-d_6): δ 9.88 (s, 1H, −NH), 9.84 (s, 1H, −NH), 8.28 (s, 1H), 7.64 (d, 4H), 7.41 (d, 2H), 7.30 (t, 2H), 7.03 (d, 1H), 6.99 (s, 1H), 6.84 (d, 2H), 3.80 (s, 6H, 2-OCH_3) ppm; ^{13}C NMR(**ESI,** Fig. S27, 100 MHz, DMSO-d_6): δ 177.56, 164.29, 162.05, 159.62, 149.00, 134.64, 129.81, 129.52, 126.32, 119.10, 118.66, 114.10, 112.70, 55.57, 32.06, 29.83, 28.55, 22.77 ppm; MS (EI) (**ESI,** Fig. S28): 404.3 (M+1), *m/z*. Elemental analysis calcd (%) for $C_{23}H_{21}N_3O_4$: C 68.47; H 5.25; N 10.42; O 15.86; found: C 68.48; H 5.26; N 10.42; O 15.84.

2.1.3.1.8. 3-Methoxy-N-(2-(4-nitrophenyl)-4-oxo-1,2-dihydroquinazolin-3(4H)-yl)benzamide (4h). The reaction between isatoic anhydride, *m*-Anisic hydrazide and 4-nitrobenzaldehyde offered compound **4h**. White powder; M.P.: 175 °C; IR(**ESI,** Fig. S29): 3447, 3225, 3022, 2298, 1733, 1638, 1579, 1395, 1283, 1202, 1192, 1133, 1120, 1045, 967, 903, 809,749, 682 cm^{-1}; ^{1}H NMR(**ESI,** Fig. S30**,** 400 MHz, DMSO-d_6): δ 9.29 (s, 1H, −NH), 8.55 (s, 1H, −NH), 8.27 (d, 6H, $J = 8$ Hz), 7.94 (s, 1H), 7.92 (s, 1H), 7.40–7.44 (m, 3H), 7.11–7.14 (m, 2H), 3.88 (s, 3H, $-OCH_3$) ppm; ^{13}C NMR(**ESI,** Fig. S31**,** 100 MHz, DMSO-d_6): δ 178.18, 153.08, 151.37, 139.84, 139.63, 128.97, 121.13, 118.96, 117.68, 111.96, 110.24, 55.97 ppm; MS (EI) (**ESI,** Fig. S32): 419.3 (M+1), *m/z*. Elemental analysis calcd (%) for $C_{22}H_{18}N_4O_5$: C 63.15; H 4.34; N 13.39; O 19.12; found: C 63.16; H 4.35; N 13.37; O 19.12.

2.2. Biology

2.2.1. In vitro methodology

2.2.1.1. Mushroom tyrosinase inhibition assay. The earlier method was followed for the examination of activity performance against mushroom tyrosinase (Sigma Chemical, USA) [29,30]. For this purpose, required quantities of mushroom tyrosinase (20 μL, 30 U/mL), phosphate buffer (140 μL, 20 mM, pH 6.8), and the inhibitor solution to be tested (20 μL) were mixed in a 96-well microplate and allowed to pre-incubation for 10 min at ambient temperature. Then, 3,4-dihydroxyphenylalanine *i.e.* L-DOPA (20 μL, 0.85 mM, Sigma Chemical, USA) was added to it followed by incubation at 25 °C for another 20 min. Later, a microplate reader (OPTI Max, Tunable) was used to record the absorbance value at 475 nm. The reference inhibitor and negative control used in this study were kojic acid and phosphate buffer, respectively. The experimental measurements were repeated three time and record their values individually. IC_{50} values were calculated by nonlinear regression using GraphPad Prism 5.0. The % Inhibition of tyrosinase was calculated using following equation (2) [29,30],

$$\text{Inhibition } (\%) = \left[\frac{B - S}{B}\right] \times 100 \tag{2}$$

where, the B and S are the absorbances for the blank and sample under studies, respectively.

2.2.1.2. Kinetic analysis for tyrosinase inhibition. On the basis of obtained IC_{50} values for synthesized compounds **4a-4h**, the most potent **4d** compound was selected for kinetic analysis. The already reported method was used to perform the series of experiments in examination of inhibition kinetics by compound **4d** [31,32]. The inhibitor concentrations for **4d** were 0.00, 0.0031, 0.0062, 0.0124 and 0.0248 μM. The variable concentration ranges are used for substrate L-DOPA from 0.0625 to 2 mM in this kinetic study. The pre-incubation and measurement time followed as per the mushroom tyrosinase inhibition assay protocol. After the addition of enzyme, the initial linear portion of absorbance used to determine the maximum initial velocity up to 5 min with 30 s time interval. The Lineweaver–Burk plot was used to examine inhibition type of enzyme in the present study. While, the secondary plot of $1/V$ versus inhibitor concentrations was studied to evaluate EI dissociation constant (*Ki*).

2.2.2. In silico analysis: computational methodology

2.2.2.1. Selection of mushroom tyrosinase structure from PDB. The Protein Data Bank (PDB) (http://www.rcsb.org) was referred to

retrieve the three dimensional (3D) structure of mushroom tyrosinase (*Agaricus bisporus*) (PDBID: 2Y9X). The protein PDBID: 2Y9X was selected on the basis of minimum resolution and absence of gaps in the residue numbers. The selected protein was energy minimized by employing conjugate gradient algorithm and amber force field in UCSF Chimera 1.10.1 [33].

2.2.2.2. Grid generation and molecular docking. There were few things adjusted in protein structure before the molecular docking experiment so as to achieve better docking results. The tyrosinase structure was prepared using the "Protein Preparation Wizard" by Maestro interface in Schrödinger Suite Release 2019-1. Initially, bond orders assigned, and hydrogen atoms were added to the protein structure. The structure of protein was minimized to reach the converged root mean square deviation (RMSD) of 0.30 Å with the OPLS_2005 force field. The co-crystallized ligands from Protein Data Bank and literature data indicate the active site of the tyrosinase enzyme [31,32,34]. The synthesized ligands **4a-4h** were sketched in 2D sketcher in Schrödinger Suite Release 2019-1 and further analyzed for the molecular docking experiment against target protein by using Glide docking protocol [35]. The experiment gave us the predicted binding energies (docking scores) and conformational positions of ligands within active region of protein. The partial flexibility and full flexibility around the active site residues for induced fit docking (IFD) approaches was performed during the docking simulations [36].

Table 2
Screening of solvent for the synthesis of quinazolinone benzamides **4a-4h**.

Sr. No.	Solvent (*v/v*)	Time (hrs.)	Yield (%)
1	Water	5	No reaction
2	Water: ethanol (9:1)	4.2	56
3	Water: ethanol (8:2)	3.8	60
4	Water: ethanol (7:3)	3.7	71
5	**Water: ethanol (6:4)**	**3.2**	**88**
6	Water: ethanol (5:5)	3.3	81
7	Water: ethanol (4:6)	3.4	79
8	Water: ethanol (3:7)	3.5	78
9	Water: ethanol (2:8)	3.7	75
10	Water: ethanol (1:9)	3.9	70
11	Ethanol	4.3	70

*Reaction condition: Isatoic anhydride (1 mmol), *m*-Anisic hydrazide (1 mmol), Benzaldehyde (1 mmol), specified solvent (10 mL), *p*-TSA as Catalyst - 10 mol %, ultrasonication at 40 °C.

3. Result and discussion

3.1. Chemistry

3.1.1. Optimization of solvent system for the synthesis of quinazolinones

The earlier synthetic route [12–14,37–49] was adopted for the synthesis of quinazolinone benzamide with some modifications such as ultrasonic reaction condition, use of *p*-TSA as catalyst and mixed solvent system. The attention was focused towards optimization of solvent by opting mixed water: ethanol system because of highly convenient, greener and harmless for synthetic methodology as witnessed through the literature survey [40–43]. Being water act as eco-friendly solvent and easily available source, our intention was to perform the reaction in water as solvent. Unfortunately, less solubility of reactants in water restricted the reaction and substantially, failed to complete even carried out for longer reaction time (Table 2, **entry 1**). Hence, we decided to inspect the reaction in mixed solvent system *i.e.* water: ethanol. Satisfyingly, we found that water: ethanol (6:4 *v:v*) (Table 2, **entry 5**) solvent system showed higher practical yield of final compound for the present transformation in short reaction time.

3.1.2. Spectroscopic studies based on absorption and fluorescence output

The spectroscopic parameters such as absorption, fluorescence emission, Stokes shift, fluorescence quantum yield and fluorescence lifetime are key the properties for any organic compound. Such properties can be investigated by using UV–visible absorption and fluorescence spectroscopy. Each of these properties examined by execution of systematic experimental conditions in three different solvents namely chloroform, dichloromethane (DCM) and methanol. The solvents were chosen for spectroscopic studies showed different polarity nature *i.e.* non-polar, polar aprotic and polar protic for chloroform, DCM and methanol, respectively. The idea behind choosing solvents with different polarity for spectroscopic analysis was to investigate the change in properties of synthesized quinazolinone benzamides **4a-4 h** at ground and excited states. Fig. 3 shows absorption spectra of synthesized quinazolinone benzamides **4a-4h** in chloroform (A), DCM (B) and methanol (C), respectively at concentration of 1 μM. From the figure, it seems that broad nature of absorption spectra of compounds **4a-4h** are bathochromically shifted when the solvent polarity increased from chloroform to methanol. The change in spectral shift and nature of absorption band observed in solvents with variable polarity is because of differences in dielectric constants and tendency to form

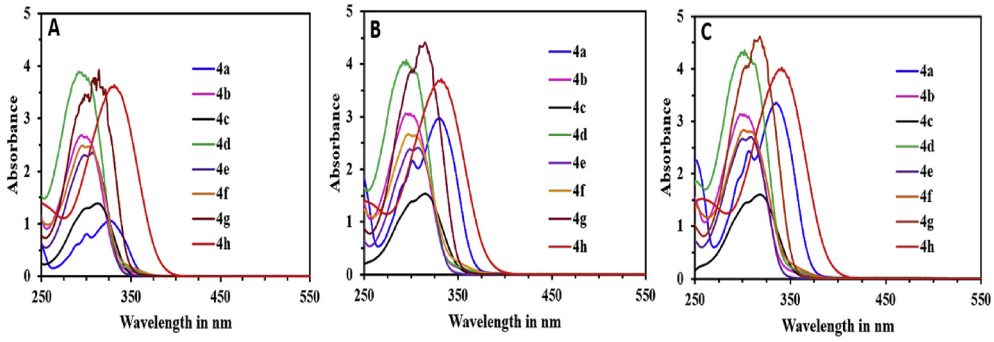

Fig. 3. Absorption spectra of compounds **4a-4h** in different solvents such as Chloroform (A), DCM (B) and Methanol (C) at 1 μM concentration.

hydrogen bonding with compound **4a-4h** by respective solvent [14,44]. The wavelength maxima for all compounds **4a-4h** observed within 291–331 nm, 296–334 nm and 303–341 nm for the solvents such as chloroform, DCM and methanol, respectively. The absorption spectra having maximum absorption wavelength for each compound in chloroform, DCM and methanol are given in Tables 3, 4 and 5, respectively.

The absorption bands occur within the wavelength range of 290–345 nm for the synthesized compounds **4a-4h** that assigned to π-π* transition originate for excitation of molecule from singlet ground state to singlet excited state [44–46]. In addition, molar extinction coefficient (ε) seems to be increased with increasing in the solvent polarity. This observation supports the absorption band signal due to π-π* electron transition [47].

Fluorescence emission spectrum of each compound was recorded at its excitation wavelength in respective solvent. The recorded fluorescence emission spectra of **4a-4 h** at concentration of 1 μM in chloroform, DCM and methanol are given as Fig. 4A, Fig. 4B and Fig. 4C, respectively. The maximum fluorescence intensity was observed in case of compounds **4d** and **4f**. While, other compounds showed significant fluorescence emission response in each solvent under studied. The smaller atomic weight of halogen atom *i.e.* fluorine (-F) and methyl group attached to para position of phenyl ring at 2 position signifies their donating contribution towards enhancement of fluorescence properties. However, other substituents on phenyl ring at 2 position for the compounds **4a, ab, 4c, 4e, 4g** and **4h** fails to produce such outputs due to their withdrawing characteristics or attachment of bulky substituent. The dependence of fluorescence emission response and bathochromic spectral shift found to be very similar as in case of absorption

Table 3
Spectroscopic properties posed by compounds **4a-4h** [1 μM] in chloroform.

Compound	λ_{abs} (nm)	ε (M^{-1} cm^{-1}) × 10^6	λ_{em} (nm)	Stokes shift (cm^{-1})	ϕ_f	τ (ns)
4a	326	1.05	402	5799.62	0.11	2.21
4b	302	2.74	400	8112.58	0.14	2.34
4c	312	1.37	407	1748.25	0.25	2.29
4d	291	3.88	416	10329.02	0.52	3.21
4e	306	2.35	412	8407.38	0.15	2.49
4f	303	2.47	414	8941.90	0.47	2.98
4g	314	3.93	407	7277.11	0.06	2.54
4h	331	3.63	382	4033.28	0.05	2.43

λ_{abs} = Maximum absorption wavelength; ε = molar extinction coefficient; λ_{em} = Wavelength at which maximum fluorescence emission occurred; ϕ_f = Fluorescence quantum yield; τ = Fluorescence lifetime.

Table 4
Spectroscopic properties posed by compounds **4a-4h** [1 μM] in DCM.

Compound	λ_{abs} (nm)	ε (M^{-1} cm^{-1}) × 10^6	λ_{em} (nm)	Stokes shift (cm^{-1})	ϕ_f	τ (ns)
4a	330	2.98	407	5733.28	0.09	2.87
4b	303	3.01	413	8790.23	0.10	2.65
4c	317	1.46	414	7391.16	0.24	2.94
4d	296	3.99	427	10364.58	0.45	3.74
4e	308	2.42	415	7770.37	0.12	2.74
4f	307	2.61	422	8976.60	0.39	3.14
4g	318	4.21	412	7174.7	0.05	2.81
4h	334	3.65	412	5668.46	0.03	2.64

λ_{abs} = Maximum absorption wavelength; ε = molar extinction coefficient; λ_{em} = Wavelength at which maximum fluorescence emission occurred; ϕ_f = Fluorescence quantum yield; τ = Fluorescence lifetime.

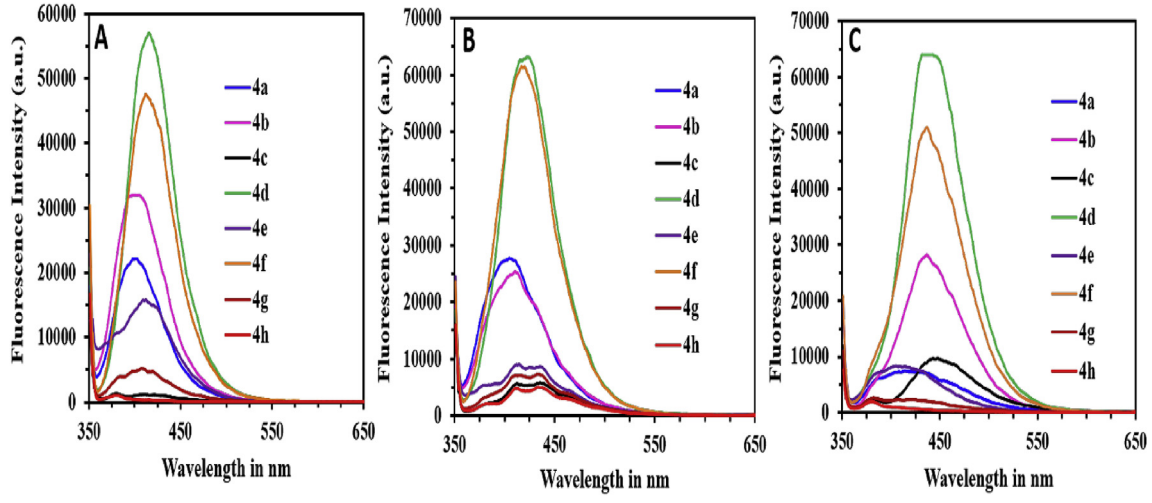

Fig. 4. Fluorescence emission spectra of compounds **4a-4h** in different solvents such as Chloroform (A), DCM (B) and Methanol (C) at 1 μM concentration.

Table 5
Spectroscopic properties posed by compounds **4a-4h** [1 μM] in methanol.

Compound	λ_{abs} (nm)	ε (M^{-1} cm^{-1}) × 10^6	λ_{em} (nm)	Stokes shift (cm^{-1})	ϕ_f	τ (ns)
4a	333	3.33	425	6056.38	0.04	3.02
4b	312	3.11	438	9220.31	0.08	2.99
4c	321	1.58	439	8373.60	0.14	3.15
4d	304	4.30	445	10422.82	0.41	4.22
4e	310	2.71	418	8339.62	0.10	3.11
4f	303	2.81	438	10172.25	0.35	3.89
4g	321	4.56	422	7455.96	0.04	3.05
4h	341	4.02	418	5402.07	0.02	3.02

λ_{abs} = Maximum absorption wavelength; ε = molar extinction coefficient; λ_{em} = Wavelength at which maximum fluorescence emission occurred; ϕ_f = Fluorescence quantum yield; τ = Fluorescence lifetime.

studies. With the increase in solvent polarity, red shift was observed in fluorescence emission spectrum of all synthesized compounds **4a-4h**. Another property explains the significant characteristics of synthesized compound is Stokes shift. Tables 3–5 illustrate that there were significant changes observed in Stokes shift values, when polarity of solvent changes. Such change in Stokes shift values clearly proposes the probability of change in structural aspects of compound's excited state level through one of the competing processes with fluorescence [44,48,49]. The stokes shift values are considerably changed for all compounds with change in the solvent polarity from chloroform to methanol except **4a** and **4g**. The comparatively same stokes shift values observed for these two compounds in chloroform and DCM solvents. The greater stabilization of the excited state level relative to the ground state level with increasing solvent polarity might be the reason behind the changes observed in stokes shift values [14,46,47]. Fluorescence quantum yield (ϕ_f) was estimated by using standard quinine sulphate method. The increasing trend was seen for fluorescence quantum yield values of compounds **4a-4h** with decreasing solvent polarity (Table 3, 4 and 5). The higher fluorescence quantum yield value was found to be 0.52, 0.45 and 0.41 for compound **4d** in chloroform, DCM and methanol, respectively. While remaining compounds shows decreasing order **4f** < **4c** < **4e** < **4b** < **4a**<**4g** < **4h** for the fluorescence quantum yield in each solvent. The lower quantum yield values observed in most polar solvent are assigned to the increase in the non-radiative pathways from the excited states of compound **4a-4h** to ground state [34,40]. The average time spend in its excited state by any fluorescent molecule is known as fluorescence lifetime (τ). The parameters which can affect the value of fluorescence lifetime of compound are solvent polarity, dielectric constant and dipole moments of the solvents used for the spectroscopic studies. The synthesized compounds **4a-4h** shows significant fluorescence lifetime values varying from 2 ns to 5 ns in different solvent used in the present experiments and given in Tables 3–5. The change in dipole moment, dielectric constant and polarity of solvents are responsible for the decrease in radiative pathways from excited state of molecule and further simultaneously increases the fluorescence lifetime values from chloroform to DCM and again in methanol for the compounds **4a-4h** [44,45,50].

3.2. Biology

3.2.1. Mushroom tyrosinase inhibition and structure activity relationship

All the synthesized quinazolinone benzamides **4a-4h** were subjected to investigate for mushroom tyrosinase inhibition activity. The compounds showed varying degrees of inhibition activity against tyrosinase enzyme. Table 6 illustrates IC_{50} values of newly synthesized compounds **4a-4h** for tyrosinase inhibitory activity. Interestingly, all compounds **4a-4h** exhibits superior tyrosinase inhibition response with much lower IC_{50} values than the standard kojic acid. In the present investigation, compounds **4a-4h** displayed lower IC_{50} values than the standard kojic acid which supports potent candidature of synthesized compounds against mushroom tyrosinase. The presence of different substituent on the aryl group at 2 position might be the reason behind varying degrees in IC_{50} values for all synthesized compounds within the range of 0.006 ± 0.074 to 1.609 ± 0.324 μM as compared to IC_{50} value 16.832 ± 1.162 μM of standard kojic acid. The involvement of electron donating and withdrawing groups on aryl ring present at 2 position of quinazolinone benzamides moiety plays an important role in efficient interaction with the target enzyme. In the present findings, compounds **4d, 4f, 4g, 4b** and **4a** bearing small molecular weight substituents on aryl ring existing at position 2 shows significantly lower IC_{50} values (0.006 ± 0.074 to 1.071 ± 0.881 μM) than the standard kojic acid (16.832 ± 1.162 μM). However, other compounds **4c** and **4e** exhibits slightly higher IC_{50} values than other synthesized compounds but comparatively lower than standard. The presence of bulky groups such as iodine and bromine in case of **4c** and **4e** may restricts their interaction with the target tyrosinase enzyme. The ascending order of tyrosinase inhibition activity for synthesized compounds based on their IC_{50} value as compared to standard kojic acid found to be **4d** < **4f** < **4g** < **4h** < **4b** < **4a**<**4c** < **4e** < kojic acid. Interestingly, all of synthesized compounds reveals considerably lower IC_{50} values than that of some earlier research reports. The alkyl hydroquinone isolated from sap of the lacquer tree (IC_{50} = 37 μM) [51], trihydroxy isoflavone (IC_{50} = 9.2 μM) [52], *trans-N*-coumaroyl tyramine (IC_{50} = 40.6 μM) [53], *cis-N*-coumaroyl tyramine (IC_{50} = 36.4 μM) [53], macrourins E isolated from morus macroura (IC_{50} = 0.39 μM) [54], tanshinone IIA (IC_{50} = 1214 μM) [55], hydroxypyridinones (IC_{50} = 12.6 & 4.0 μM) [56], thiocarbazones (IC_{50} = 0.35–0.44 mM) [57] and kojic acid analogue ($IC_{50} = 1.35 \pm 2.15$ μM) [58] are some of synthetic and natural sources used as tyrosinase inhibitors. Those are comparable IC_{50} values with the synthesized quinazolinone derivatives **4a-4h** in the present investigation. This literature survey shows that the lower IC_{50} values possessed by the synthesized

Table 6
IC_{50} values of newly synthesized quinazolinone benzamides **4a-4h** for Tyrosinase inhibition activity.

Compound	Tyrosinase activity $IC_{50} \pm SEM$ (μM)
4a	1.071 ± 0.881
4b	0.411 ± 0.012
4c	1.419 ± 0.962
4d	0.006 ± 0.074
4e	1.609 ± 0.324
4f	0.057 ± 0.096
4g	0.239 ± 0.054
4h	0.347 ± 0.051
Kojic acid	16.832 ± 1.162

*SEM= Standard error of the mean; values are expressed in mean ± SEM.

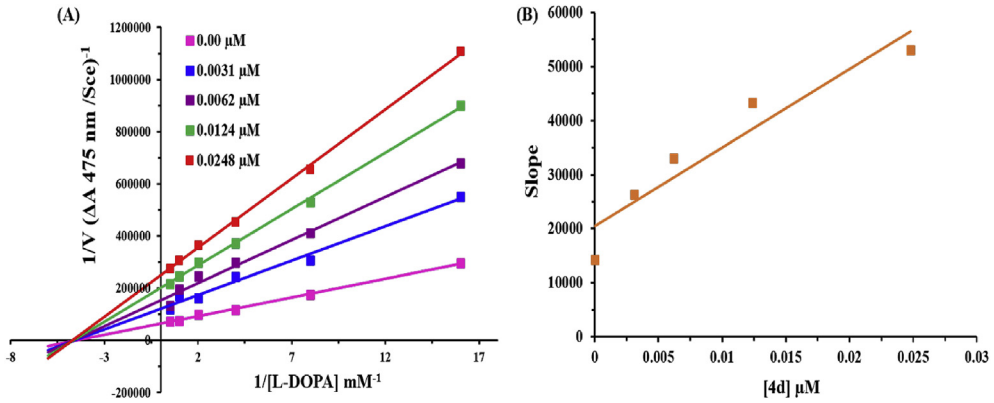

Fig. 5. (A) Lineweaver–Burk plot for inhibition of tyrosinase in presence of Compound 4d; Concentrations of **4d** were 0.00, 0.0031, 0.0062, 0.0124 and 0.0248 µM, respectively. Substrate L-DOPA concentrations were 0.0625, 0.125, 0.25, 0.5, 1 and 2 mM, respectively. (B) Plot of the slope versus inhibitor **4d** concentrations to determine inhibition constant. The lines were drawn using linear least squares fit.

Table 7
Kinetic parameters of the mushroom tyrosinase for L-DOPA activity in presence of various concentrations of **4d**.

Concentration of 4d (µM)	V_{max} (ΔA/Sec)	K_m (mM)	Inhibition Type	*Ki* (µM)
0.00	$1.36{,}667 \times 10^{-5}$	0.2	Non-competitive	0.014
0.0031	$8.36{,}364 \times 10^{-6}$	0.2		
0.0062	$7.51{,}515 \times 10^{-6}$	0.2		
0.0124	$4.59{,}771 \times 10^{-6}$	0.2		
0.0248	$3.63{,}142 \times 10^{-6}$	0.2		

*V_{max} is the reaction velocity, K_m is the Michaelis-Menten constant, and *Ki* is the EI dissociation constant.

compounds **4a-4h** indicate its higher potency against tyrosinase inhibition than reported compounds. In an overall, results accomplished that compounds **4a-4h** shows superior tyrosinase inhibition activity and could be useful as potent templates for drug design in pharmaceutical industries.

3.2.2. Kinetic analysis

To understand the inhibitory mechanism of synthesized compounds **4a-4h** on tyrosinase enzyme, the kinetic study was performed. Based on our IC_{50} results, we were selected the most potent compound **4d** for the determination of inhibition type and inhibition constant. The kinetic results of the enzyme plotted as Lineweaver-Burk plot of 1/V against 1/[S] in the presence of different inhibitor concentrations results in a series of straight lines as shown in Fig. 5 (A). The results of kinetic study and plot showed that compound **4d** intersected within the second quadrant. While, V_{max} decreased with increasing doses of inhibitors and no change in K_m value. This kinetic behavior specifies that compound **4d** inhibit the tyrosinase enzyme non-competitively to form the enzyme-inhibitor complex. The enzyme inhibitor dissociation constant (*Ki*) was calculated by plotting the slope against concentration of inhibitor given as Fig. 5B. The kinetic parameters of the mushroom tyrosinase for L-DOPA activity in the presence of various concentrations of **4d** are given as Table 7.

3.2.3. Chemoinformatics properties and Lipinski's rule of five (RO5) validation

The chemoinformatics properties of all the synthesized compounds (**4a-4h**) were predicted by using computational tool Molinspiration followed by validation of Lipinski rule of five (RO5) using Molsoft. This rule states that molecular mass and log*P* values should be less than 500 g/mol and 5, respectively. Moreover, the compounds should possess no greater than 10 HBA and 5 HBD, respectively. Earlier research work indicates that higher values of HBA and HBD results in poor drug permeability. Pleasingly, all the compounds **4a-4h** obey RO5 rule including compound **4c** even it has little higher molecular weight than 500 g/mol. The surface sum of all polar atoms within a molecule is considered as polar surface area (PSA) which frequently utilized to predict the drug ability in cell permeation. The predicted results showed that all synthesized compounds possess less values of PSA than previous reports [59,60]. Thus, predicted results on chemoinformatics parameters for all compound showed that synthesized compounds **4a-4h** fall in standard range which indicate their potent oral bioactivity behavior. The estimated chemoinformatics properties of synthesized quinazolinone benzamides (**4a-4h**) listed in Table 8. The molecular flexibility is considered by their assessment of number of rotational bonds (nrotb). Any single bond beside the ring structure of compound and bounded to heavy non-hydrogen atom is called as rotatable bond. The high rotational energy barrier of C–N bond led to exclude it from such estimations. The number of rotational

Table 8
Chemoinformatics properties of synthesized quinazolinone benzamides **4a-4h**.

Ligands	Mol.wt. (g/mol)	No. HBA	No. HBD	Log*P*	PSA (A^2)	Mol. Vol (A^3)	nrotb	Drug Score
4a	389	4	3	3.51	77	376	4	1.27
4b	373	3	2	3.89	61	363	4	0.75
4c	515	3	2	4.16	61	369	4	1.03
4d	391	4	3	4.31	77	407	4	1.40
4e	452	3	2	4.74	61	385	4	1.11
4f	387	3	2	4.29	61	384	4	1.30
4g	403	4	2	3.98	68	395	5	1.06
4h	418	5	2	3.62	99	389	5	0.77

bonds less than 10 suggest compound's good oral bioavailability in rat. Our experimental values of nrotb (Table 8) for all the synthesized compounds fall in standard range which illustrates their good oral bioavailability behavior. The parameters such as hydrophobicity, molecule size and flexibility, hydrogen bonding characteristics along with presence of various pharmacophoric features are collectively known as drug score of target compound [61]. The generated results for our synthesized all compounds showed that compounds **4a-4h** exhibits good drug score values, which indicates its drug-resemblance behavior. All compounds showed predicted positive values of drug scores which are mentioned in Table 8.

3.2.4. Molecular docking analysis

3.2.4.1. Binding energy evaluation of synthesized compounds 4a-4h. To predict the best-fitted conformational position of synthesized ligands **4a-4h** within the active region of target protein, the generated docked complexes were analyzed on the basis of Glide docking energy values (kcal/mol) and bonding interaction (hydrogen/hydrophobic) behavior. The lowest binding energy value depicts the best conformational position of ligand within the active region of target protein. The docking results showed that all the synthesized ligands **4a-4h** were bind within the active site of target protein with different conformational poses and energy values. Fig. 6 (A) illustrates **t**he binding pattern of all synthesized compounds **4a-4h** showed similar conformational behavior within the active region of target protein. Moreover, the energy values of all compounds **4a-4h** were resemble to each other and graphically presented as Fig. 6 (B). The basic skeleton of all the synthesized compounds **4a-4h** found to be similar except the substituents present on aryl ring of quinazolinone. Therefore, obtained binding energy values are close to each other with no big difference.

3.2.4.2. Binding analysis of ligands against tyrosinase. Based on *in vitro* results, **4d** docking complex was evaluated to understand their binding conformational analysis within active site of target protein. In detail, docking analysis results interpreted two π-π interactions in **4d** docking complex. The 3D and 2D depictions of most active compound **4d** are shown in Fig. 7 (A) and Fig. 7 (B), respectively. The benzene ring with substituent fluorine and aryl moiety of benzamide site interacts through π-π interactions at Phe264 and Hie244, respectively with target tyrosinase protein. Literature data also ensured and supports our *in vitro* tyrosinase inhibition activity and *in silico* molecular docking analysis results by stating the importance of these residues in bonding with other

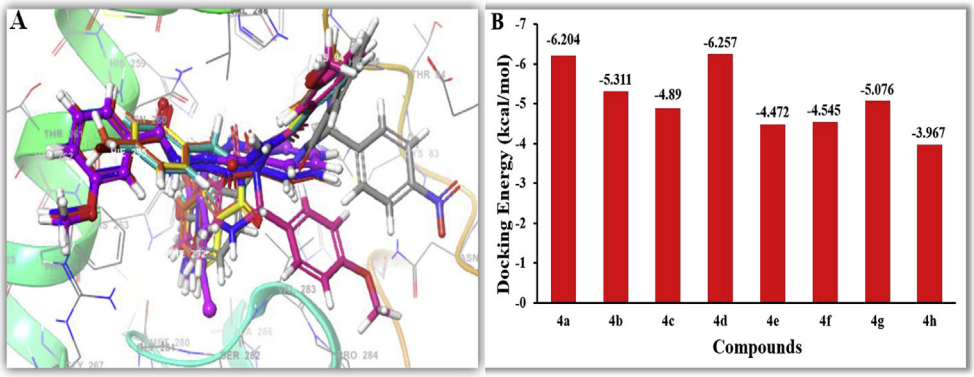

Fig. 6. Docking energy complexes of synthesized quinazolinone benzamides **4a-4h** within the active region of target protein (A) along with binding energy values (kcal/mol) (B).

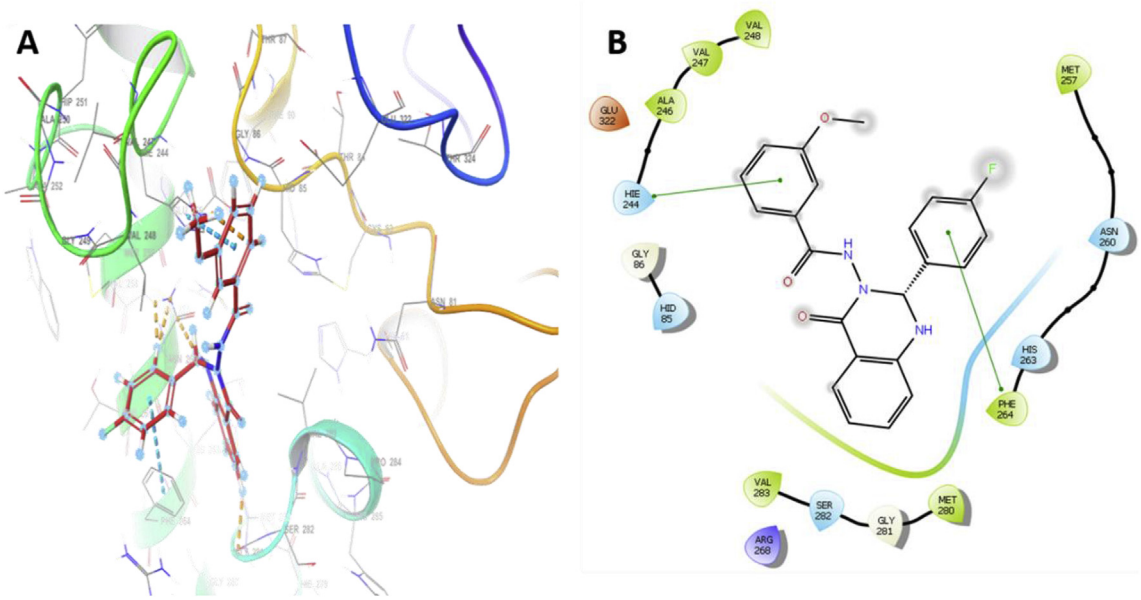

Fig. 7. 3D (A) and 2D (B) docking depictions of **4d** complex against tyrosinase.

tyrosinase inhibitors [29,32–34]. The docking complexes of synthesized compounds **4a**, **4b**, **4c**, **4e**, **4f**, **4g** and **4h** are given as supporting information (ESI, Figs. S33–S39).

4. Conclusion

The newly synthesized quinazolinone benzamides **4a-4h** has been successfully characterized at molecular scale using IR, NMR, Mass spectroscopies and elemental analysis. The comparative studies based on absorption and fluorescence properties such as absorbance, emission, molar extinction coefficient, fluorescence quantum yield, Stokes shift and fluorescence lifetime for each compounds **4a-4h** reveal outstanding spectroscopic properties in three different solvents. The comparative syntax about the changes observed in such properties in compounds **4a-4h** have been discussed in detail. In addition, synthesized compounds **4a-4h** shows excellent inhibitory activity against tyrosinase enzyme. The *in vitro* analysis indicates excellent tyrosinase inhibition activity response for all compounds possessing lower IC_{50} values within range of 0.006 ± 0.074 to 1.609 ± 0.324 μM as compared to the standard kojic acid (IC_{50} value 16.832 ± 1.162 μM). While, *in silico* molecular docking investigation is in support of *in vitro* findings. In an overall, compounds **4d** and **4f** show excellent absorption and fluorescence-based properties along with extremely lower IC_{50} values for tyrosinase inhibition (IC_{50} value for 4d = 0.006 ± 0.074 μM and IC_{50} value for 4d = 0.057 ± 0.096 μM). The newly synthesized quinazolinone derivatives, employment of mild reaction conditions, use of water: ethanol as a green solvent, operational simplicity, excellent practical yield of products, easy isolation of products, use of ultrasonication rather than harsh heating conditions and potent tyrosinase activity shown by synthesized derivatives are remarkable, novel and advantageous characteristics of the present synthetic methodology. From the comprehensive results in the present investigation, it concludes that compounds **4a-4h** can be used as biomarker in cell imaging and serve as template in molecular drug design for the development of potent inhibitor against tyrosinase enzyme.

Conflicts of interest

Authors declares that there is no conflict of interests.

Acknowledgement

This research has been performed as a cooperation project of “Enhancement of Korea Chemical Bank” and supported by the Korea Research Institute of Chemical Technology (KRICT).

Appendix A. Supplementary data

Supplementary data to this article can be found online at https://doi.org/10.1016/j.molstruc.2019.126915.

References

[1] V. Alagarsamy, U.S. Pathak, Synthesis and antihypertensive activity of novel 3-benzyl-2-substituted-3H-[1,2,4]triazolo[5,1-b]quinazolin-9-ones, Bioorg. Med. Chem. 15 (2007) 3457–3462. https://doi.org/10.1016/j.bmc.2007.03.007.

[2] L. Xu, W.A. Russu, Molecular docking and synthesis of novel quinazoline analogues as inhibitors of transcription factors NF-kB activation and their anticancer activities, Bioorg. Med. Chem. 21 (2013) 540–546. https://doi.org/10.1016/j.bmc.2012.10.051.

[3] C. Ma, Y. Li, S. Niu, H. Zhang, X. Liu, Y. Che, N-Hydroxypyridones, phenylhydrazones, and a quinazolinone from Isaria farinose, J. Nat. Prod. 74 (2011) 32–37. https://doi.org/10.1021/np100568w.

[4] Y. Zhuang, X. Teng, Y. Wang, P. Liu, G. Li, W. Zhu, New quinazolinone alkaloidswithin rare amino acid residue from coral-associated fungus, Aspergillus versicolorLCJ-5–4, Org. Lett. 13 (2011) 1130–1133. https://doi.org/10.1021/ol103164n.

[5] D.J. Conolly, D. Cusack, T.P. O'Sullivan, P.J. Guiry, Synthesis of quinazolinones and quinazolines, Tetrahedron 61 (2005) 10153–10202. https://doi.org/10.1016/j.tet.2005.07.010.

[6] S.B. Mhaske, N.P. Argade, The chemistry of recently isolated naturally occurring quinazolinone alkaloids, Tetrahedron 62 (2006) 9787–9826. https://doi.org/10.1016/j.tet.2006.07.098.

[7] P.C. Sharma, G. Kaur, R. Pahwa, A. Sharma, H. Rajak, Quinazolinone analogs as potential therapeutic agents, Curr. Med. Chem. 18 (2011) 4786–4812. https://doi/10.2174/092986711797535326.

[8] M. Dabiri, P. Salehi, S. Otokesh, M. Baghbanzadeh, G. Kozehgary, A.A. Mohammadi, Efficient synthesis of mono- and disubstituted 2,3-dihydroquinazolin-4(1H)-ones using $KAl(SO_4)_2 \cdot 12H_2O$ as a reusable catalyst in water and ethanol, Tetrahedron Lett. 46 (2005) 6123–6126. https://doi.org/10.1016/j.tetlet.2005.06.157.

[9] V. Alagarsamy, S. Murugesan, Synthesis and pharmacological evaluation of some3-(4-methoxyphenyl)-2-substitutedamino-quinazolin-4(3H)-ones as analgesic and antiinflammatory agents, Chem. Pharm. Bull. 55 (2007) 76–80. https://doi/10.1248/cpb.55.76.

[10] Z. Wang, M. Wang, X. Yao, Y. Li, J. Tan, L. Wang, W. Qiao, Y. Geng, Y. Liu, Q. Wang, Design, synthesis, and antiviral activity of novel quinazolinones, Eur. J. Med. Chem. 53 (2012) 275–282. https://doi.org/10.1016/j.ejmech.2012.04.010.

[11] S. Tiwari, V. Mujalda, V. Sharma, P. Saxena, M. Shrivastava, Synthesis and evaluationof Schiff's base of 4-quinazolinone analogues as antimicrobial agents, Asian J. Pharmaceut. Clin. Res. 5 (2012) 98–100. https://innovareacademics.in/journal/ajpcr/Vol5Issue1/715.pdf.

[12] A.A. Mohammadi, S. Askari, H. Rohi, A.A. Soorki, Design, synthesis, and antibacterial evaluation of some novel 3′-(Phenylamino)-1′Hspiro[indoline-3,2′-quinazoline]-2,4′(3′H)-dione derivatives, Synth. Commun. 44 (2014) 457–467. https://doi.org/10.1080/00397911.2013.796992.

[13] R. Ghorbani-Vaghei, A. Shahriari, Y. Maghbooli, J. Mahmoudi, Efficient synthesis of novel quinazoline-4(1H)-one derivatives by N-halosulfonamides, Res. Chem. Intermed. 43 (2017) 983–993. https://doi.org/10.1007/s11164-016-2678-5.

[14] F.A. Cabrera-Rivera, J. Escalante, H. Morales-Rojas, D.F. Zigler, R.D. Schmidt, L.E. Jarocha, M.D.E. Forbes, Photophysical properties of 2,3-dihydroquinazolin-4(1H)-one derivatives, J. Photochem. Photobiol. A Chem. 294 (2014) 31–37. https://doi.org/10.1016/j.jphotochem.2014.07.005.

[15] S.P. Anthony, Polymorph-dependent solid-state fluorescence and selective metal-ion-sensor properties of 2-(2-hydroxyphenyl)-4(3H)-quinazolinone, Chem. Asian J. 7 (2012) 374–379. https://doi.org/10.1002/asia.201100832.

[16] X.B. Zhang, G. Cheng, W.J. Zhang, G.L. Shen, R.Q. Yu, A fluorescent chemical sensor for Fe^{3+} based on blocking of intramolecular proton transfer of a quinazolinone derivative, Talanta 71 (2017) 171–177. https://doi.org/10.1016/j.talanta.2006.03.036.

[17] T.V. Trashakhova, E.V. Nosova, M.S. Valova, P.A. Slepukhin, G.N. Lipunova, V.N. Charushin, Synthesis and photophysical properties of 2-styrylquinazolin-4-ones, Russ. J. Org. Chem. 47 (2011) 748–755. https://doi.org/10.1134/S1070428011050150.

[18] E.V. Nosova, T.V. Stupina, G.N. Lipunova, M.S. Valova, P.A. Slepukhin, V.N. Charushin, 3-Phenyl/Pyridinyl derivatives of trans-2-(aryl/heteryl)vinyl-3H-quinazolin-4-ones: synthesis and fluorescent properties, Int. J. Org. Chem. 2 (2012) 56–63. https://doi/10.4236/ijoc.2012.21010.

[19] M.T.H. Khan, Heterocyclic compounds against the enzyme tyrosinase essential for melanin production: biochemical features of inhibition, in: M.T.H. Khan (Ed.), Bioactive Heterocycles III. Topics in Heterocyclic Chemistry, vol. 9, Springer, Berlin, Heidelberg, 2007. https://doi.org/10.1007/7081_2007_077.

[20] (a) T. Pillaiyar, M. Manickam, V. Namasivayam, Skin whitening agents: medicinal chemistry perspective of tyrosinase inhibitors, J. Enzym. Inhib. Med. Chem. 32 (2017) 403–425. https://doi.org/10.1080/14756366.2016.1256882;
(b) M. Rafiq, M. Saleem, M. Hanif, S.K. Kang, S.Y. Seo, K.H. Lee, Synthesis, structural elucidation and bioevaluation of 4-amino-1,2,4-triazole-3-thione's Schiff base derivatives, Arch Pharm. Res. (Seoul) 39 (2016) 161–171. https://doi.org/10.1007/s12272-015-0688-2.

[21] A. Vontzalidou, G. Zoidis, E. Chaita, M. Makropoulou, N. Aligiannis, G. Lambrinidis, E. Mikros, A.L. Skaltsounis, Design, synthesis and molecular studies of dihydrostilbene derivatives as potent tyrosinase inhibitors, Bioorg. Med. Chem. Lett 22 (2012) 5523–5526. https://doi.org/10.1016/j.bmcl.2012.07.029.

[22] K. Ohguchi, T. Tanaka, T. Kido, K. Baba, M. Iinuma, K. Matsumoto, Y. Akao, Y. Nozawa, Effects of hydroxystilbene derivatives on tyrosinase activity, Biochem. Biophys. Res. Commun. 307 (2003) 861–863. https://doi.org/10.1016/S0006-291X(03)01284-1.

[23] I. Tessari, M. Bisaglia, F. Valle, B. Saori, E. Bergantino, S. Mammi, L. Bubacco, The reaction of alpha-synuclein with tyrosinase: possible implications for Parkinson disease, J. Biol. Chem. 283 (2008) 16808–16817. https://doi/10.1074/jbc.M709014200.

[24] (a) S. Zolghadria, A. Bahramia, M.T.H. Khan, J. Munoz-Munoz, F. Garcia-Molina, F. Garcia-Canovas, A.A. Saboury, A comprehensive review on tyrosinase inhibitors, J. Enzym. Inhib. Med. Chem. 34 (2019) 279–309. https://doi.org/10.1080/14756366.2018.1545767;
(b) W.Y. Huang, Y.Z. Cai, Y. Zhang, Natural phenolic compounds from medicinal herbs and dietary plants: potential use for cancer prevention, Nutr.

Cancer 62 (2010) 1–20. https://doi.org/10.1080/01635580903191585;
(c) J. Liu, F. Wu, L. Chen, L. Zhao, Z. Zhao, M. Wang, S. Lei, Biological evaluation of coumarin derivatives as mushroom tyrosinase inhibitors, Food Chem. 135 (2012) 2872–2878. https://doi.org/10.1016/j.foodchem.2012.07.055.

[25] (a) B. De, I. Adhikari, A. Nandy, A. Saha, B.B. Goswami, In silico modelling of azole derivatives with tyrosinase inhibition ability: application of the models for activity prediction of new compounds, Comput. Biol. Chem. 74 (2018) 105–114. https://doi.org/10.1016/j.compbiolchem.2018.03.007;
(b) S.S. Gawande, S.C. Warangkar, B.P. Bandgar, C.N. Khobragade, Synthesis of new heterocyclic hybrids based on pyrazole and thiazolidinone scaffolds as potent inhibitors of tyrosinase, Bioorg. Med. Chem. 21 (2013) 2772–2777. https://doi.org/10.1016/j.bmc.2012.12.053;
(c) K. Sakuma, M. Ogawa, K. Sugibayashi, K. Yamada, K. Yamamoto, Relationship between tyrosinase inhibitory action and oxidation-reduction potential of cosmetic whitening ingredients and phenol derivatives, Arch Pharm. Res. (Seoul) 22 (1999) 335–339. https://link.springer.com/content/pdf/10.1007/BF02979054.pdf.

[26] (a) N. Gheibi, A.A. Saboury, K. Haghbeen, F. Rajaei, A.A. Pahlevan, Dual effects of aliphatic carboxylic acids on cresolase and catecholase reactions of mushroom tyrosinase, J. Enzym. Inhib. Med. Chem. 24 (2009) 1076–1081. https://doi.org/10.1080/14756360802632658;
(b) L. Saghaie, M. Pourfarzam, A. Fassihi, B. Sartippour, Synthesis and tyrosinase inhibitory properties of some novel derivatives of kojic acid, Res. Pharm. Sci. 8 (2013) 233–242. https://www.ncbi.nlm.nih.gov/pmc/articles/PMC3757588/;
(c) K.I. Nihei, I. Kubo, Substituent effect of benzaldehydes on tyrosinase inhibition, Plant Physiol. Biochem. 112 (2017) 278–282. https://doi.org/10.1016/j.plaphy.2017.01.009.

[27] A.B. Ormond, H.S. Freeman, Effects of substituents on the photophysical properties of symmetrical porphyrins, vol. 96, 2013, pp. 440–448. https://doi.org/10.1016/j.dyepig.2012.09.011.

[28] M. Rojkiewicz, P. Kus, P. Kozub, M. Kempa, The synthesis of new potential photosensitizers [1]. Part 2. Tetrakis- (hydroxyphenyl)porphyrins with long alkyl chain in the molecule, Dyes Pigments 99 (2013) 627–635. https://doi.org/10.1016/j.dyepig.2013.06.029.

[29] Q. Abbas, H. Raza, M. Hassan, A.R. Phull, S.J. Kim, S.Y. Seo, Acetazolamide inhibits the level of tyrosinase and melanin: an enzyme kinetic, in vitro, in vivo and in silico studies, Chem. Biodivers. 14 (2017), e1700117. https://doi.org/10.1002/cbdv.201700117.

[30] A.R.S. Butt, M.A. Abbasi, S.Z. Siddiqui, H. Raza, M. Hassan, S.A.A. Shah, M. Shahid, S.Y. Seo, Synthesis and structure-activity relationship of tyrosinase inhibiting novel bi-heterocyclic acetamides: mechanistic insights through enzyme inhibition, kinetics and computational studies, Bioorg. Chem. 86 (2019) 459–472. https://doi.org/10.1016/j.bioorg.2019.01.036.

[31] F.A. Larik, A. Saeed, P.A. Channar, U. Muqadar, Q. Abbas, M. Hassan, S.Y. Seo, M. Bolte, Design, synthesis, kinetic mechanism and molecular docking studies of novel 1-pentanoyl-3-arylthioureas as inhibitors of mushroom tyrosinase and free radical scavengers, Eur. J. Med. Chem. 141 (2017) 273–281. https://doi.org/10.1016/j.ejmech.2017.09.059.

[32] A. Saeed, P.A. Mahesar, P.A. Channar, Q. Abbas, F.A. Larik, M. Hassan, H. Raza, S.Y. Seo, Synthesis, molecular docking studies of coumarinyl-pyrazolinyl substituted thiazoles as non-competitive inhibitors of mushroom tyrosinase, Bioorg. Chem. 74 (2017) 187–196. https://doi.org/10.1016/j.bioorg.2017.08.002.

[33] E.F. Pettersen, T.D. Goddard, C.C. Huang, G.S. Couch, D.M. Greenblatt, E.C. Meng, T.E. Ferrin, UCSF Chimera – a visualization system for exploratory research and analysis, J. Comput. Chem. 25 (2006) 1605–1612. https://doi.org/10.1002/jcc.20084.

[34] M. Hassan, Z. Ashraf, Q. Abbas, H. Raza, S.Y. Seo, Exploration of novel human tyrosinase inhibitors by molecular modeling, docking and simulation studies, Interdiscip. Sci. 10 (2018) 68–80. https://doi.org/10.1007/s12539-016-0171-x.

[35] R.A. Friesner, R.B. Murphy, M.P. Repasky, L.L. Frye, J.R. Greenwood, T.A. Halgren, P.C. Sanschagrin, D.T. Mainz, Extra precision Glide: docking and scoring incorporating a model of hydrophobic enclosure for protein-ligand complexes, J. Med. Chem. 49 (2006) 6177–6196. https://doi.org/10.1021/jm051256o.

[36] R. Farid, T. Day, R.A. Friesner, R.A. Pearlstein, New insights about HERG blockade obtained from protein modeling, potential energy mapping, and docking studies, Bioorg. Med. Chem. 14 (2006) 3160–3173. https://doi.org/10.1016/j.bmc.2005.12.032.

[37] B.H. Chen, J.T. Li, G.F. Chen, Efficient synthesis of 2,3-disubstituted-2,3-dihydroquinazolin-4(1H)-ones catalyzed by dodecylbenzenesulfonic acid in aqueous media under ultrasound irradiation, Ultrason. Sonochem. 23 (2015) 59–65. https://doi.org/10.1016/j.ultsonch.2014.08.024.

[38] X. Zhu, S.R. Kang, L. Xia, J. Lee, N. Basavegowda, Y.R. Lee, Efficient Cu(OTf)2 -catalyzed synthesis of novel and diverse 2,3-dihydroquinazolin-4(1H)-ones, Mol. Divers. 19 (2015) 67–75. https://doi.org/10.1007/s11030-014-9557-z.

[39] Z.H. Zhang, H.Y. Lu, S.H. Yang, J.W. Gao, Synthesis of 2,3-dihydroquinazolin-4(1H)-ones by three-component coupling of isatoic anhydride, amines, and aldehydes catalyzed by magnetic Fe_3O_4 nanoparticles in water, J. Comb. Chem. 12 (2010) 643–646. https://doi.org/10.1021/cc100047j.

[40] N.C. Dige, J.D. Patil, D.M. Pore, Dicationic 1,3-Bis(1-methyl-1H-imidazole-3-ium) propane copper(I) dibromate : novel heterogeneous catalyst for 1,3-dipolar cyclo-addition, Catal. Lett. 147 (2017) 301–309. https://doi.org/10.1007/s10562-016-1942-z.

[41] N.C. Dige, P.G. Mahajan, D.M. Pore, Serendipitous formation of novel class of dichromeno pyrano pyrimidinone derivatives possessing anti-tubercular activity against M. tuberculosis H37Rv, Med. Chem. Res. 27 (2018) 224–233. https://doi.org/10.1007/s00044-017-2062-z.

[42] N.C. Dige, S.N. Korade, D.M. Pore, Design of task-specific ionic liquid, 1-(ethylaceto acetate)-1-(2-hydroxyethyl) piperidinium tetrachloroaluminate for multicomponent synthesis of 3,3′-disubstituted oxindoles, Res. Chem. Intermed. 43 (2017) 7029–7040. https://doi.org/10.1007/s11164-017-3034-0.

[43] N.C. Dige, D.M. Pore, Green aspect for multicomponent synthesis of spiro[4*H*-indeno[1,2-b]pyridine-4,3′-[3*H*]indoles], syn. Comm. 45 (2015) 2498–2510. https://doi.org/10.1080/00397911.2015.1092551.

[44] P.G. Mahajan, N.C. Dige, B.D. Vanjare, H. Raza, M. Hassan, S.Y. Seo, S.K. Hong, K.H. Lee, Synthesis and studies of fluorescein based derivatives for their OpticalProperties, urease inhibition and molecular docking, J. Fluoresc. 28 (2018) 1305–1315. https://doi.org/10.1007/s10895-018-2291-7.

[45] B.D. Vanjare, P.G. Mahajan, M. Hassan, H. Raza, S.Y. Seo, S.K. Hong, K.H. Lee, Design, synthesis, photophysical properties, biological estimation and molecular docking studies of novel schiff base derivatives as potential urease inhibitors, J. Fluoresc. 28 (2018) 1295–1304. https://doi.org/10.1007/s10895-018-2289-1.

[46] P.G. Mahajan, N.C. Dige, S.B. Suryawanshi, D.K. Dalavi, A.A. Kamble, D.P. Bhopate, A.N. Kadam, V.V. Kondalkar, G.B. Kolekar, S.R. Patil, FRET between riboflavin and 9-anthraldehyde based fluorescent organic nanoparticles possessing antibacterial activity, J. Fluoresc. 28 (2018) 207–215. https://doi.org/10.1007/s10895-017-2183-2.

[47] P. Crews, J. Rodriguez, M. Jaspars, Organic Structure Analysis, Oxford University Press, Inc, USA, 1998, pp. 349–374.

[48] P.L. Muińo, P.R. Callis, Solvent effects on the fluorescence quenching of tryptophan by amides via Electron transfer. Experimental and computational studies, J. Phys. Chem. B 113 (2009) 2572–2577. https://doi.org/10.1021/jp711513b.

[49] M.A. Haidekker, T.P. Brady, D. Lichlyter, E.A. Theodorakis, Effect of solvent polarity and solvent viscosity on the fluorescence properties of molecular rotors and related probes, Bioorg. Chem. 33 (2005) 415–425. https://doi.org/10.1016/j.bioorg.2005.07.005.

[50] P.G. Mahajan, N.C. Dige, B.D. Vanjare, A.R. Phull, S.J. Kim, S.K. Hong, K.H. Lee, Synthesis, photophysical properties and application of new porphyrin derivatives for use in photodynamic therapy and cell imaging, J. Fluoresc. 28 (2018) 871–882. https://doi.org/10.1007/s10895-018-2264-x.

[51] Y.R. Chen, R. Chiou, T.Y. Lin, C. Huang, W. Tang, S. Chen, S. Lin, Identification of an alkylhydroquinone from Rhus succedanea as an inhibitor of tyrosinase and melanogenesis, J. Agric. Food Chem. 57 (2009) 2200–2205. https://doi.org/10.1021/jf802617a.

[52] T.S. Chang, H.Y. Ding, H.C. Lin, Identifying 6,7,4'-trihydroxyisoflavone as a potent tyrosinase inhibitor, Biosci. Biotechnol. Biochem. 69 (2005) 1999–2001. https://doi.org/10.1271/bbb.69.1999.

[53] H.H. Yang, K.E. Oh, Y.H. Jo, H.H. Ahn, Q. Liu, A. Turk, J.Y. Jang, B.Y. Hwang, K.Y. Lee, M.K. Lee, Characterization of tyrosinase inhibitory constituents from the aerial parts of Humulus japonicus using LC-MS/MS coupled online assay, Bioorg. Med. Chem. 26 (2018) 509–515. https://doi.org/10.1016/j.bmc.2017.12.011.

[54] Y. Wang, L. Xu, W. Gao, L. Niu, C. Huang, P. Yang, X. Hu, Isoprenylated phenolic compounds from Morus macroura as potent tyrosinase inhibitors, Planta Med. 84 (2018) 336–343. https://doi.org/10.1055/s-0043-121698.

[55] Y.L. Wang, G. Hu, Q. Zhang, Y.X. Yang, Q.Q. Li, Y.J. Hu, H. Chen, F.Q. Yang, Screening and characterizing tyrosinase inhibitors from Salvia miltiorrhiza and Carthamus tinctorius by spectrum-effect relationship analysis and molecular docking, J. Anal. Methods Chem. 2018 (2018) 1–10. https://doi.org/10.1155/2018/2141389.

[56] D.F. Li, P.P. Hu, M.S. Liu, X.L. Kong, J.C. Zhang, R.C. Hider, T. Zhou, Design and synthesis of hydroxypyridinone-l-phenylalanine conjugates as potential tyrosinase inhibitors, J. Agric. Food Chem. 61 (2013) 6597–6603. https://doi.org/10.1021/jf401585f.

[57] M.A. Soares, M.A. Almeida, C. Marins-Goulart, O.A. Chaves, A. Echevarria, M. de Oliveira, Thiosemicarbazones as inhibitors of tyrosinase enzyme, Bioorg. Med. Chem. Lett 27 (2017) 3546–3550. https://doi.org/10.1016/j.bmcl.2017.05.057.

[58] W. Xie, H. Zhang, J. He, J. Zhang, Q. Yu, C. Luo, S. Li, Synthesis and biological evaluation of novel hydroxybenzaldehyde-based kojic acid analogues as inhibitors of mushroom tyrosinase, Bioorg. Med. Chem. Lett 27 (2017) 530–532. https://doi.org/10.1016/j.bmcl.2016.12.027.

[59] R.U. Kadam, N. Roy, Recent trends in drug-likeness prediction: a comprehensive review of in silico methods, Indian J. Pharm. Sci. 69 (2007) 609–615, https://doi.org/10.4103/0250-474X.38464.

[60] M.R. Bhosale, L.D. Khillare, J.R. Mali, A.P. Sarkate, D.K. Lokwani, S.V. Tiwari, DIPEAc promoted one-pot synthesis of dihydropyrido[2,3-*d*:6,5-*d'*]dipyrimidinetetraone and pyrimido[4,5-*d*]pyrimidine derivatives as potent tyrosinase inhibitors and anticancer agents: in vitro screening, molecular docking and ADMET predictions, New J. Chem. 42 (2018) 18621–18632, https://doi.org/10.1039/c8nj04622k.

[61] W. Walters, P. Ajay, M.A. Murcko, Recognizing molecules with drug-like properties, Curr. Opin. Chem. Biol. 3 (1999) 384–387. https://doi.org/10.1016/S1367-5931(99)80058-1.